Crosslinked, Electrospun Chitosan–Poly(ethylene oxide) Nanofiber Mats

Jennifer L. Vondran,[1] Wei Sun,[2] Caroline L. Schauer[1]

[1]*Department of Materials Science and Engineering, Drexel University, 3141 Chestnut Street, Philadelphia, Pennsylvania 19104*
[2]*Department of Mechanical Engineering and Mechanics, Drexel University, 3141 Chestnut Street, Philadelphia, Pennsylvania 19104*

Received 25 September 2007; accepted 20 December 2007
DOI 10.1002/app.28107
Published online 11 April 2008 in Wiley InterScience (www.interscience.wiley.com).

ABSTRACT: Mechanical characterization of nanofiber mats is an underexplored area in biomaterial engineering. In this study, a chitosan–poly(ethylene oxide) copolymer blend was electrospun and crosslinked with glutaraldehyde (GA) for various time periods. The tensile and compressive mechanical integrity of the nanofibers was analyzed with increasing exposure to vapor crosslinking. Solubility, scanning electron microscopy characterization, Fourier transform infrared, uniaxial tensile tests, and nanoindentation analyses were used to identify these trends. The mechanical studies confirmed that the GA vapor crosslinking increased the stiffness and decreased the ductility of the electrospun mats. Increased exposure time to crosslinking led to changes in the mat surface color and resistance to dissolution. Scanning electron microscopy fiber counts verified that exposure to GA vapor crosslinking increased the average fiber diameter. By the use of vapor phase deposition, mechanical properties continued to change throughout the study. The crosslinking exposure time could be chosen to accommodate *in vivo* mechanical loading. © 2008 Wiley Periodicals, Inc. J Appl Polym Sci 109: 968–975, 2008

Key words: biopolymers; crosslinking; fibers; mechanical properties

INTRODUCTION

Natural polymers are preferred over synthetic polymers for tissue engineering because of their low immunogenicity, nontoxic degradation, and improved biocompatibility and bioresorbability.[1] Chitosan, the N-deacetylated derivative of chitin (at least 60% deacetylated), is found in the shells of crustaceans and arthropods and also in fungi and yeast. Basic in nature, chitosan has applications in wound healing and tissue repair, drug delivery, antimicrobial resistance, metal-ion adsorption, and cell adhesion.[2–6] Chitosan is a copolymer of 2-amino-2-deoxy-D-glucopyranose and 2-acetamido-2-deoxy-D-glucopyranose monomeric units with β-(1–4) glycosidic linkages. The increased availability of amines combined with the hydroxyl groups on highly deacetylated versions of chitosan improves its modification capacity, allowing for the addition of growth factors and cell signaling molecules in specific tissue engineering applications.[7] Poly(ethylene oxide) (PEO) is a biocompatible, nontoxic, inert polymer that can interact with chitosan to improve the charge-carrying capacity of electrospinning blends. PEO also lowers the viscosity of highly concentrated chitosan solutions,[1] and a homogeneous, noncovalent polymeric blend forms upon mixing.

The polymer processing technique of electrospinning has been demonstrated to have potential uses in tissue engineering,[8–16] especially for cartilage regeneration,[17,18] because of the high surface area to volume ratio, interconnectivity, pore void volume, potential dynamicity, and nanometer dimensions of the three-dimensional fibers that it produces.[18] To perform a simple electrospinning experiment, one would need a syringe (or pipette) to store the solution or blend, a syringe needle, a voltage supply, and a grounded collector target (Fig. 1). Electrospinning was patented by Formhaals in 1934 (U.S. Pat. 1,975,504) and relies on electrostatic repulsions in polymer solutions or blends (which are introduced by an external, applied electric field) to overcome the surface tension within the blends. The formation of a Taylor cone at the apex of the syringe needle signifies the repulsion of electrostatic forces between the surface tension and the applied electric field strength. This indicates that the blend is capable of electrospinning. Once the surface tension is overcome, the jet undergoes a nonaxisymmetric whipping instability until it is collected on a grounded target. The target distance and voltage can be modi-

Correspondence to: C. L. Schauer (cschauer@coe.drexel.edu).

Contract grant sponsors: Lois and Max Beren Foundation, ASM International, National Society of Professional Engineers, International Association of Plastics Distributors, Delaware Valley Engineer's Council and Society of Women Engineers.

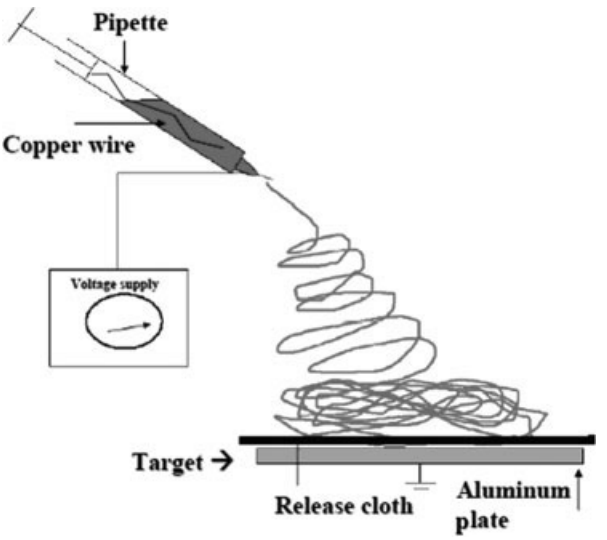

Figure 1 Schematic of the electrospinning setup.

fied to allow the solvent to evaporate so that only solidified, submicrometer fibers are collected. The nanofibrillar, nonwoven, elastomeric mesh has characteristics of the cartilage extracellular matrix (ECM) environment (i.e., collagen fibrils) that would be suitable for cellular attachment and differentiation.[9,16]

Challenges arise with electrospinning chitosan in nontoxic, neutral pH solvents. This is a criterion for tissue engineering applications to minimize the occurrence of toxic solvent residue on or in the nanofibers. The cationic nature of chitosan (protonation of the amine residue on C-2) contributes to its solubility in low-volume-percentage, acidic solvents (pH < 5.0), including hydrochloric, formic, acetic, lactic, and citric acids. Even though chitosan can dissolve in a low-percentage acid, it has been challenging to electrospin. Chitosan by itself has been electrospun in 90% acetic acid (AcOH),[19] trifluoroacetic acid, trifluoroacetic acid/methylene chloride, and poly(vinyl alcohol) solutions.[20–22] It has been reported that the addition of PEO to chitosan blends improves the solubility and charge-carrying capacity in low-volume-percentage AcOH solutions.[23] A higher degree of deacetylation of chitosan increases its maximum tensile strength because of the higher crystallinity of the uninterrupted chains of glucosamine units.[24] Therefore, a highly deacetylated version of chitosan, combined with PEO and electrospun with a weak acid, would be an improvement for tissue engineering function over existing chitosan nanofibers.

Specifically, chitosan nanofibers are candidates for cartilage tissue engineering applications because of their morphology and chemical resemblance to natural ECM. While serving as temporary cell matrices, polymeric chitosan–PEO nanofibers would transmit the tensile loads, and the glucosamine chemistry of chitosan would shield the compressive stresses; this is similar to the role of fibrous collagens and glycosaminoglycans/proteoglycans in natural ECM.[18,25] The mechanical integrity of natural polymers, specifically chitosan, must be improved before implantation into the body.[26,27] Crosslinking electrospun chitosan fibers would be a viable option.

Chitosan crosslinking agents include glutaraldehyde (GA),[28–31] sulfuric acid,[32] genipin,[33] oxidized glucose,[34] hexamethylene 1,6-di(aminocarboxysulfonate),[35] and resimene.[36] Chitosan readily crosslinks with hyaluronic acid,[37,38] genipin,[39,40] chondroitin sulfate,[41,42] heparin,[43,44] and alginate[45] to improve biocompatibility, cell adhesion, and proliferation.

Crosslinking GA with chitosan has been suggested to improve the mechanical integrity of chitosan,[46] through the formation of iminic (C=N) bonds, via Schiff's base reaction between chitosan and GA.[47–49] Figure 2 depicts iminic bond formation from Schiff's base reaction. The degree of deacetylation of chitosan affects the covalent crosslinking activity of GA.[47] A highly deacetylated chitosan is favorable for crosslinking because the free amino groups on carbon 2 of chitosan react with the carbonyl on GA.[24]

Material properties of nanofibers have recently become the focus of many studies.[14] The literature reports how rheological properties of chitosan–PEO blends (surface tension, conductivity, and viscosity) and the optimization of electric field processing variables contribute to nanofiber formation.[1,19,50] Fourier transform infrared (FTIR) and differential scanning calorimetry data have also been presented,[23] but to date there has been no mention of mechanical property analysis. In our laboratory, the tensile properties of GA-crosslinked chitosan fibers have been studied, but only at a single time period of crosslinking.[22] No compression behavior has been ascertained.

Therefore, the aim of this study was to electrospin a biocompatible, biomimetic scaffold with improved mechanical properties introduced via vapor phase deposition crosslinking. To accomplish this, a chitosan–PEO blend was electrospun and crosslinked with GA for various time periods to determine

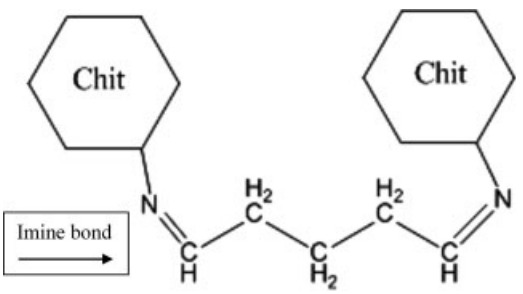

Figure 2 Schiff's base reaction forms an imine bond between chitosan (Chit) and GA.

whether the tensile and compressive mechanical integrity of the nanofibers could be altered with increasing exposure to vapor crosslinking. Solubility, scanning electron microscopy (SEM) characterization, FTIR, uniaxial tensile tests, and nanoindentation analyses were used to identify these trends.

EXPERIMENTAL

Materials

All compounds were used as received. Ninety percent deacetylated pharmaceutical-grade chitosan was obtained from the Naval Research Laboratory (Washington, DC). PEO [weight-average molecular weight (M_w) = 600 kDa], GA (50 wt % solution in water), sodium hydroxide (NaOH; solid), and AcOH (99.7%; American Chemical Society reagent) were purchased from Sigma–Aldrich (St. Louis, MO). All solutions were used at room temperature; solutions containing water used deionized and distilled water.

Blend preparation

A 4% (w/v) chitosan–PEO blend (100 mL) with a mass ratio of 1 : 1 was prepared by the addition of 2 g of chitosan with 2 g of PEO to 96 mL of a 2% AcOH solution (pH = 2.63). Magnetic stirring mixed the blend at room temperature overnight; the blend was stored at 9°C.

Electrospinning

The electrospinning apparatus is depicted in Figure 1. Constant stirring with a magnetic stirring bar brought the blend to room temperature before electrospinning. The blend was pipetted into a 5.75″ borosilicate glass Pasteur pipette (Fisher Scientific, Pittsburgh, PA) and attached to a ring stand. A Gamma High Voltage ES series power supply (Gamma High Voltage Research, Inc., Ormond Beach, FL) applied 20 kV of positive charge via an alligator clip to a copper wire, which was inserted into the open end of the pipette. The collector consisted of an aluminum plate covered with release cloth attached to an aluminum plate with double-sided electric tape. Release cloth was used on the target to easily remove the nanofiber mats. The power supply applied negative charge to the aluminum plate via a second alligator clip. The needle-to-collector distance was 15 cm. Temperature and relative humidity readings of the electrospinning chamber were monitored for each sample with a thermohygrometer (Fisher Scientific). A painter lamp and dehumidifier, placed inside the chamber, improved ambient conditions. Throughout the electrospinning process, temperatures ranged from 29 to 33°C, and the relative humidity ranged from 18 to 38%.

Crosslinking

Nanofiber mats of various sizes were placed on two empty vapor containers with base dimensions of 12.7 cm × 10.7 cm and 12.2 cm × 8.5 cm at room temperature in a ventilated hood. The nanofibers were not removed from the release cloth. Five milliliters of room-temperature 50% GA was pipetted into the base of each container and evenly dispersed. GA crosslinked with the nanofibers through vapor deposition as the GA vaporized to the top of the container, where the samples were located. Nanofiber mats were crosslinked for 0 min (control), 10 min, 30 min, 1 h, 2 h, 5 h, 10 h, 15 h, and 20 h. The crosslinked nanofiber mats were stored in plastic bags in a desiccator.

Solubility

Nanofiber mats (1 cm^2) crosslinked for 0 min, 30 min, 2 h, and 10 h were tested for their solubilities in 60 mm × 15 mm Falcon tissue culture dishes (Becton Dickinson Labware, Bedford, MA). The dishes contained 10 mL of a 1*M* NaOH solution, 1*M* AcOH solution, or neutral deionized and distilled water. The solubility behavior of the samples was observed at 15 min and 72 h. One sample was tested under each condition.

SEM

One control mat and one 10-h crosslinking mat were purged with argon and sputter-coated with platinum for 30 s with a Denton Vacuum Desk II sputtering machine (Morrestown, NJ). Samples were viewed with a Zeiss Supra 50/VP field emission scanning electron microscope.

FTIR

For each crosslinking time point, three measurements were taken in the diffused reflectance mode of a Digilab Excalibur series UMA 600 IR microscopy spectrometer (Canton, MA). One respective spectrum from each crosslinking time point was analyzed. All spectra were taken in the spectral range of 4000–500 cm^{-1} by an accumulation of 256 scans with a resolution of 2 cm^{-1} and, depending on the sample, various degrees of sensitivity.

Nanoindentation

One mat from each crosslinking time period (removed from release cloth) was tested on an MTS

Nano Indenter XP (Eden Prairie, MN) according to the XP basic hardness, modulus, tip calibration, and displacement control modified method. Modulus and hardness data were analyzed with Testworks4 in the XP basic method. Testing was conducted at room temperature. A 13.5-μm-radius spherical tip was used because the tested samples were polymers (softer materials), and elastic properties were primarily targeted. Surface roughness error was minimized. All samples were tested in a batch mode. Silica was used as a standard for calibration purposes before testing. Testworks4 fixed Poisson's ratio at 0.180. After averaging of the thickness of the fiber mats (no release cloth) with a caliper, which was found to be 30–50 μm, a 200 nm/s displacement rate was selected to a maximum tip depth limit of 1000 nm. The tip was held at a peak holding time of 1 s. The tip indented each sample only once. The time to load and unload was kept at 5 s. Each test was taken to 99% of unloading. Twenty indents of four random five by one arrays, spaced 10 μm apart, were taken per sample.

Uniaxial tensile testing

An Instron 4442 mechanical tester (Norwood, MA) was used to measure the applied load versus the nanofiber mat extension to calculate stress–strain curves for three samples (5-mm width × 20-mm length) from each respective crosslinking time period. A 5 N load cell was used to test the samples at a rate of 0.05 mm/s to 10% strain to mimic *in vivo* cell-mediated contraction. Each sample was weighed and then mounted in tensile grips, which were covered with a layer of sandpaper to ensure a good grip during the test. The gauge length was set to 10 mm. The testing was conducted at room temperature. All raw data acquired from the tensile test samples were normalized by consideration of each sample's unique areal density.

Tensile data were normalized because the mats had different weights and thicknesses. GA is included in the normalized data, but the density of GA is ignored because the amount of GA deposition is unknown. Any change in mechanical behavior was assumed to have been contributed by the GA vapor deposition.

The mechanical optimization study assumed heterogeneous vapor deposition crosslinking due to the anisotropic physical appearance of the crosslinked mats and a random orientation of nanofibers. It was also assumed that the fiber samples were created under the same ambient conditions (29–33°C), and the mechanical analysis was a bulk property analysis of the fibers. The mechanical properties of single nanofibers were not studied. The authors hypothesize that vapor deposition crosslinking increases the stiffness and decreases the ductility of the nanofiber mats.

RESULTS AND DISCUSSION

Solubility

Solubility is a qualitative indicator of structural and chemical changes in a modified material. The control samples, with zero exposure to vapor deposition crosslinking, fully dissolved in all three solvents: acidic, basic, and neutral. This behavior was observed at both time points, 15 min and 72 h. The samples exposed to vapor deposition crosslinking, however, were resistant to dissolution, having an increased ability to absorb liquid. The crosslinked samples also turned slightly brown in color as opposed to the white color of the control fibers. Increased exposure time to GA deposition darkened the color of the mats. The crosslinked samples exhibited the same behavior in all three solvents at both time points.

SEM

A nanofiber mat not exposed to GA vapor deposition was compared to a nanofiber mat under exposure to vapor deposition for 10 h to determine whether there was a change in the average nanofiber diameter size. An object is considered to have nanodimensions if one length scale of the object is less than 100 nm. SEM images of two samples, magnified at 60,000×, are depicted in Figure 3. The scale bar in the images represents 800 nm. The images illustrate dense networks of nonwoven fibers. Fifty fiber diameters were counted in each sample to determine the average fiber diameter. The control sample had an average fiber diameter of 41.38 ± 9.14 nm. The mat crosslinked for 10 h had an average fiber diameter of

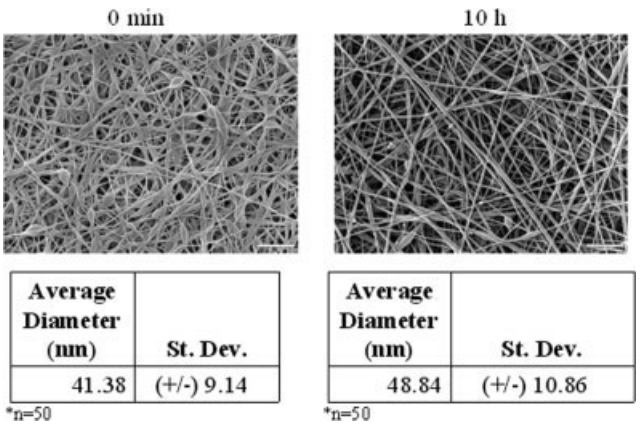

Figure 3 SEM images of noncrosslinked and crosslinked nanofiber mats. The images were taken at a magnification of 60,000×. Scale bars in the images represent 800 nm.

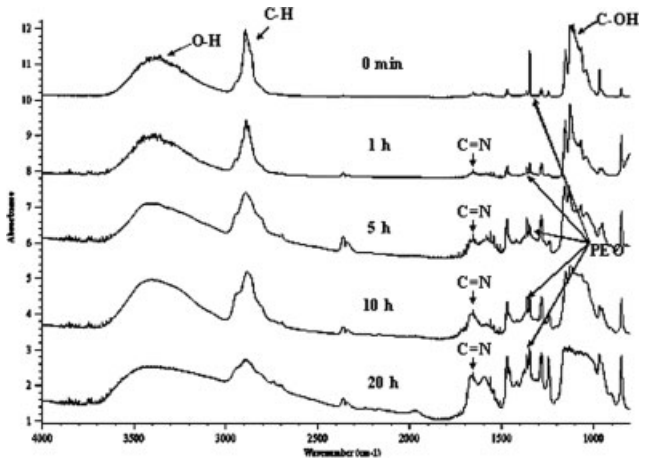

Figure 4 Comparison of FTIR spectra of nanofiber mats.

48.84 ± 10.86 nm. Standard deviations are high because the electrostatic process of ''pulling'' on the blend and the instability of the whipping jet produce randomly sized fibers. The data indicate that vapor deposition crosslinking slightly increases the average diameter size. Previously, GA crosslinking studies have been performed on chitosan nanofibers. According to Schiffman and Schauer,[22] chitosan nanofibers were crosslinked via GA vapor deposition for at least 24 h. The authors reported an average fiber diameter increase of 26.9% for high-M_w chitosan and increases as high as 423% for low-M_w chitosan.

FTIR

In the copolymer chitosan–PEO blend, it is hypothesized that intermolecular hydrogen bonding occurs between the primary hydroxyl groups of chitosan and either the protonated hydroxyl end groups on PEO or the oxygen in the C—O—C PEO chain. It is also possible that water is hydrogen-bound to the primary hydroxyl groups of chitosan and to the oxygen in the C—O—C PEO chain.

FTIR spectra of a control mat and mats crosslinked for 1, 5, 10, and 20 h are displayed in Figure 4. Several chemical groups of chitosan (O—H, C—H, and C—OH stretches) and peaks for PEO are also displayed. Theoretically, as vapor deposition exposure lengthens, the carbon-to-nitrogen ratio should increase as the amine-to-imine bond ratio decreases. These assumptions are verified by the FTIR spectra. The C—H peak at 2877 cm^{-1} widens as the vapor deposition exposure lengthens. The literature reports an imine bond (C=N) from the Schiff base reaction between chitosan and GA in FTIR spectra at 1620–1660 cm^{-1}.[46] Figure 4 indicates that as vapor exposure increases, peak areas from 1653 to 1664 cm^{-1} increase as well. Because the crosslinking reaction was primarily a Schiff base reaction, carbonyl groups were not observed in the FTIR spectra at 1720–1730 cm^{-1}, which would indicate Michael adduct crosslinking.[22]

Uniaxial tensile testing

The specific stress [σ (g/tex)] of the fibers was calculated with the following equation:

$$\sigma(\mathrm{g/tex}) = [F(\mathrm{converted\ N})/w(\mathrm{mm})]/\delta(\mathrm{g/m^2})$$

where 1 N is equal to 101.971 gram-force units, N is the applied load (N) reported from the Instron 442 software, F is the gram-force (applied load in newtons converted to gram-force units), w is the sample width (5 mm), and δ is the areal density (mass of the sample divided by the sample area; the sample area was 20 mm × 5 mm).

σ (g/tex) was converted to the stress [σ (MPa)] by

$$\sigma(\mathrm{MPa}) = 9.8 \times \sigma(\mathrm{g/tex}) \times \mu(\mathrm{g/cm^3})$$

where μ is the density of the nanofiber mat [0.5 × 1.13 g/cm^3 (PEO) + 0.5 × 1.562 g/cm^3 (chitosan); taken from the *Polymer Handbook*].[55] The electrospun mat was assumed to be half-composed of pharmaceutical-grade chitosan and half-composed of PEO.

The strain (ε) was calculated with the following equation:

$$\varepsilon = [x(\mathrm{s}) \times \kappa(\mathrm{mm/s})]/l(\mathrm{mm})$$

where x is the time value reported from the Instron 442 software, κ is the extension rate (0.05 mm/s), and l is the gauge length of the sample (10 mm).

Tensile testing quantifies the overall fiber interconnectivity strength of the fiber mat. A graph of representative stress–strain curves from each time point is depicted in Figure 5. The tensile elastic modulus for

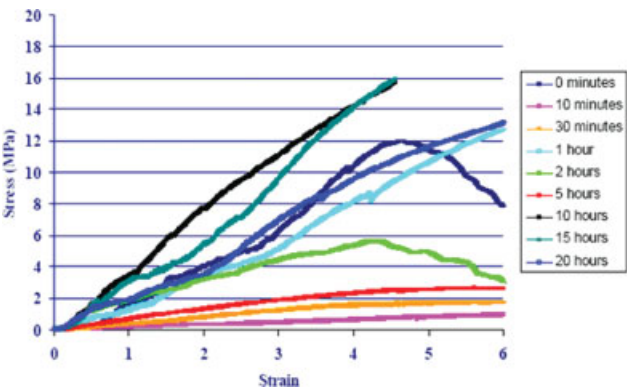

Figure 5 Stress–strain curves taken to 10% strain at an extension rate of 0.05 mm/s. [Color figure can be viewed in the online issue, which is available at www.interscience.wiley.com.]

TABLE I
Elastic Modulus Averages from Uniaxial Tensile Tests

Time	Average tensile elastic modulus (MPa)	Standard deviation (±)
0 min	1.32	0.389
10 min	0.135	0.029
30 min	0.368	0.009
1 h	1.51	0.718
2 h	1.82	0.715
5 h	0.747	0.891
10 h	2.79	0.826
15 h	2.57	1.12
20 h	2.13	0.05

three samples from each crosslinking time point was found by calculation of the slope of the linear part of the stress–strain curve, and the results are displayed in Table I. The results indicate that the tensile elastic modulus reached a maximum after 10 h of GA vapor deposition, reaching as high as 2.787 MPa. Initially, after 10 min of crosslinking, there was a structural weakening of the fiber mat, as the tensile elastic modulus fell from 1.3162 (control value at 0 h) to 0.1348 MPa. This may have been caused by initial solvent exchange within the fiber mat, initial instabilities arising from decreased crystallinity after low degrees of crosslinking,[49] and the initial destabilizing presence of the rigid iminic bond over the more flexible chitosan amine. The addition of imines leads to a decrease in the primary amine content and an overall increase in carbon and hydrogen.[47] This may affect the intramolecular electrostatic repulsions and the slightly expanded coil conformation of the chitosan chain.[51]

As the vapor deposition time increases, there is a stiffening of the chitosan chain due to the formation of iminic bonds with GA. The weak, self-associated network of chitosan is replaced by a covalent network, and the mat becomes brittle as the crosslinking density increases.[51] The tensile elastic modulus surpasses the control modulus after 1 h of crosslinking. At 5 h, there is a critical drop in the tensile elastic modulus to 0.75 MPa. Two independently prepared batches, with a sample size of n = 3 per batch, displayed this same drop in the tensile elastic modulus. This negative occurrence is negated because there is a continued increase in the tensile elastic modulus except at 5 h of crosslinking, and the tensile elastic modulus reaches its highest point at 10 h. There is no significant difference in the sample weight between all samples tested. The authors theorize that there is a drop in the tensile elastic modulus at 5 h because of the increase in vapor deposition on the fibers from 0 min to 5 h. As vapor deposition increases, the fiber samples become more like an amorphous elastomer, and a glass-to-rubber transition may occur. Because of polymer chain entanglement, the chitosan chains may have restricted mobility. After 10 h, the network reaches its strongest point, and greater amounts of vapor deposition decrease the tensile elastic modulus slightly. It is noted that all tensile elastic modulus values after 10 h of crosslinking are still higher than all other values before 10 h of crosslinking.

Nanoindentation

Nanoindentation quantifies bulk polymer behavior in the compression mode and is commonly referred to as depth-sensing indentation. It determines the modes of deformation of a material, which are plastic (permanent) and elastic (reversible). Nanoindentation measures load directly and displacement indirectly to calculate the compressive elastic modulus and hardness. Hardness is the calculated ratio of the maximum load and the residual indentation area of the tip (based on the contact displacement and the shape of the tip); hardness changes as a function of penetration depth in the sample. Hardness is the pressure at which a material plastically deforms. The compressive elastic modulus is measured at the beginning of the indenter unloading. Nanoindentation is less destructive than tensile testing, has a loading resolution less than 50 nN, and a spatial resolution less than 0.1 nm.

A graph of nanoindentation load/displacement curves is depicted in Figure 6. The compressive elastic modulus and hardness values from each crosslinking time point are depicted in Table II. The MTS Nano Indenter Testworks4 software uses stored information about the tip's geometry and mechanical properties and a user-defined Poisson's ratio as inputs for modulus and hardness calculations. Load

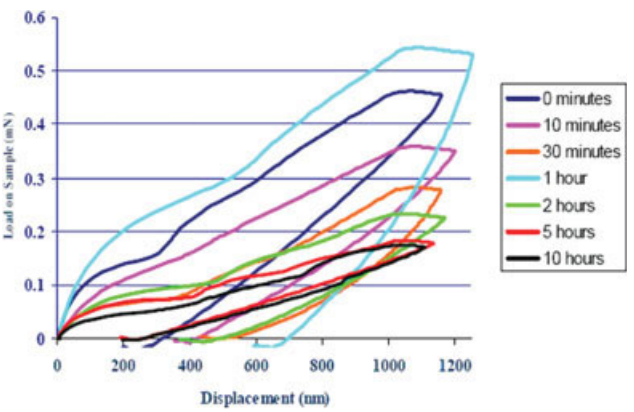

Figure 6 Nanoindentation load/displacement curves. [Color figure can be viewed in the online issue, which is available at www.interscience.wiley.com.]

TABLE II
Elastic Modulus Averages from Nanoindentation Tests

Time	Average compressive elastic modulus (MPa)	Standard deviation (±)	Hardness (MPa)
0 min	9.46	69.9	5
10 min	84.2	106.3	6
30 min	98.6	92.7	6
1 h	141.2	314	7
2 h	55.8	14.3	8
5 h	37.2	6.5	5
10 h	35.6	13.1	5

is measured as a function of contact displacement, and modulus and hardness are then calculated from data generated by the load/displacement curves. The curves represent average values for each crosslinking time point. The indent tip was held for only 1 s to not promote creep and a viscoelastic response from the polymer. If, however, there had been a viscoelastic response in any way, this would have affected the contact displacement of the tip as the tip unloaded from the sample; this may explain the large standard deviations observed in Table II. Overall, the compressive elastic moduli were much greater than the GA crosslinked tensile elastic moduli. A higher compressive elastic modulus would be useful in cartilage regeneration applications because of the high-impact loads withstood by the articular cartilage in knees or hips.[52] The compressive elastic modulus decreased only slightly from the control group to 10 min of crosslinking. The negative trend then shifted, and the compressive elastic modulus increased until there was a maximum compressive elastic modulus of 141 MPa after 1 h of GA vapor deposition. Average hardness values reached a maximum of 8 MPa after 2 h and leveled off at 5 MPa after 10 h of crosslinking. After 10 h, the fiber mats were too brittle to withstand compressive loading. Because engineered articular cartilage should have a compressive elastic modulus exceeding 1 MPa in compression, the 2-h sample could be used as a cartilage replacement.[52]

The shapes of the nanoindentation load/displacement curves are very similar, indicating similar structural behavior. The areas under the curves are very different, however, correlating to the differences in sample strength and sample resistance to unloading. As the indenter penetrates the top, less dense layers of the fiber mat (due to surface charge repulsion of the individual fibers after electrospinning), nanofibers realign and act together to be stronger as the density of the fiber layers increase at deeper depths. Interconnecting pore sizes are smaller in deeper layers. Top, less dense nanofiber layers would be ideal for cellular movement and contraction.

CONCLUSIONS

This study has verified that structural properties of the nanofiber mats change after GA vapor deposition crosslinking, becoming more brittle and less ductile. The polymer nanofibers are affected, losing crystallinity during the process of crosslinking. As reported in the literature, reduced crystallinity due to crosslinking may lead to an increase in the availability of chelating groups, increased hydrophilicity, and adsorption capacity for metal cations.[53] Low-volume exposure to GA vapor deposition may find useful applications in the areas of chelation, hydrophilization, and metal-cation adsorption. Other studies, involving films, have verified that GA solution crosslinking decreases the extensibility and increases the stress at break for gelatin films.[54] Future studies will quantify the degree of crosslinking and changes in the C/N ratio as the ratio of amine to imine bonds decreases. To minimize the range of standard deviations, a more homogeneous method of crosslinking needs to be developed. The crosslinking time can be chosen according to the desired mechanical properties of nanofiber mats, depending on which types of *in vivo* loading will occur in the environment of the scaffold.

Drexel University's Materials Characterization Facilities are acknowledged for the use of the scanning electron microscope, nanoindenter, and Fourier transform infrared apparatus. Many thanks are extended to Aaron Sakulich and Jessica Schiffman for their assistance with the scanning electron microscopy imaging and Adrian Gurga for his technical assistance with the nanoindenter. The authors thank Tony Lowman for his permission to use the Instron apparatus and Jon Thomas for his technical assistance.

References

1. Bhattarai, N.; Edmondson, D.; Veiseh, O.; Matsen, F. A.; Zhang, M. Biomaterials 2005, 26, 6176.
2. Krajewska B. Sep Purificat Technol 2005, 41, 305.
3. Koide, S. S. Nutr Res 1998, 18, 1091.
4. Qin, Y. Med Device Technol 2004, January, 34.
5. Marguerite, R. Prog Polym Sci 2006, 31, 603.
6. Rabea, E. I.; Badawy, M. E.; Stevens, C. V.; Smagghe, G.; Steurbaut, W. Biomacromolecules 2003, 4, 1457.
7. Kumar, M. N. V. R. React Funct Polym 2000, 46, 1.
8. Ma, Z.; Kotaki, M.; Inai, R.; Ramakrishna, S. Tissue Eng 2005, 11, 101.
9. Li, W.-J.; Laurencin, C. T.; Caterson, E. J.; Tuan, R. S.; Ko, F. K. J Biomed Mater Res A 2002, 60, 613.
10. Li, M.; Mondrinos, M. J.; Gandhi, M. R.; Ko, F. K.; Weiss, A. S.; Lelkes, P. I. Biomaterials 2005, 26, 5999.
11. Lannutti, J.; Reneker, D.; Ma, T.; Tomasko, D.; Farson, D. Mater Sci Eng C 2007, 27, 504.
12. Smith, L. A.; Ma, P. X. Colloids Surf B 2004, 39, 125.
13. Han, D.; Gouma, P.-I. Nanomed: Nanotechnol Biol Med 2006, 2, 37.
14. Frenot, A.; Chronakis, I. S. Curr Opin Colloid Interface Sci 2003, 8, 64.

15. Pham, Q. P.; Sharma, U.; Mikos, A. G. Tissue Eng 2006, 12, 1197.
16. Nair, L. S.; Bhattacharyya, S.; Laurencin, C.T. Exp Opin Biol Ther 2004, 4, 659.
17. Subramanian, A.; Vu, D.; Larsen, G. F.; Lin, H.-Y. J Biomater Sci Polym Ed 2005, 16, 861.
18. Li, W.-J.; Tuli, R.; Okafor, C.; Derfoul, A.; Danielson, K. G.; Hall, D. J.; Tuan, R. S. Biomaterials 2005, 26, 599.
19. Geng, X.; Kwon, O.-H.; Jang, J. Biomaterials 2005, 26, 5427.
20. Ohkawa, K.; Cha, D.; Kim, H.; Nishida, A.; Yamamoto, H. Rapid Commun 2004, 25, 1600.
21. Li, L.; Hsieh, Y.-L. Carbohydr Res 2006, 341, 374.
22. Schiffman, J. D.; Schauer, C. L. Biomacromolecules 2007, 8, 594.
23. Duan, B.; Dong, C.; Yuan, X.; Yao, K. J Biomat Sci Polym Ed 2004, 15, 797.
24. Adekogbe, I.; Ghanem, A. Biomaterials 2005, 26, 7241.
25. Li, Z.; Zhang, M. J Biomed Mater Res A 2005, 75A, 485.
26. Subramanian, A.; Lin, H.-Y. J Biomed Mater Res A 2005, 75A, 742.
27. Neto, C. G. T.; Dantas, T. N. C.; Fonseca, J. L. C.; Pereira, M. R. Carbohydr Res 2005, 340, 2630.
28. Sridhar, S.; Susheela, G.; Reddy, G. J.; Khan, A. A. Polym Int 2001, 50, 1156.
29. Krajewska, B. J Chem Technol Biotechnol 2001, 76, 636.
30. Musale, D.A.; Kumar, A. Sep Purificat Technol 2000, 21, 27.
31. Wang, X.-P.; Feng, Y.-F.; Shen, Z.-Q. J Appl Polym Sci 2000, 75, 740.
32. Ge, J.; Cui, Y.; Yan, Y.; Jiang, W. J Membr Sci 2000, 165, 75.
33. Mi, F.-L.; Tan, Y.-C.; Liang, H.-F.; Sung, H.-W. Biomaterials 2002, 23, 181.
34. Li, F.; Liu, W. G.; Yao, K. D. Biomaterials 2002, 23, 343.
35. Welsh, E. R.; Schauer, C. L.; Qadri, S. B.; Price, R. R. Biomacromolecules 2002, 3, 1370.
36. Schauer, C. L.; Chen, M.-S.; Chatterley, M.; Eisemann, K.; Welsh, E. R.; Price, R. R.; Schoen, P. E.; Ligler, F. S. Thin Solid Films 2003, 434, 250.
37. Feng, Q.; Zeng, G.; Yang, P.; Wang, W.; Cai, J. Colloids Surf A 2005, 257, 85.
38. Yamane, S.; Iwasaki, N.; Majima, T.; Funakoshi, T.; Masuko, T.; Harada, K.; Minami, A.; Monde, K.; Nishimura, S.-I. Biomaterials 2005, 26, 611.
39. Butler, M. F.; Ng, Y.-F.; Pudney, P. D. A. J Polym Sci Part A: Polym Chem 2003, 41, 3941.
40. Mi, F.-L.; Shyu, S.-S.; Peng, C.-K. J Polym Sci Part A: Polym Chem 2005, 43, 1985.
41. Denuziere, A.; Ferrier, D.; Damour, O.; Domard, A. Biomaterials 1998, 19, 1275.
42. Denuziere, A.; Ferrier, D.; Domard, A. Carbohydr Polym 1996, 29, 317.
43. Kweon, D.-K.; Song, S.-B.; Park, Y.-Y. Biomaterials 2003, 24, 1595.
44. Wang, X. H.; Li, D. P.; Wang, W. J.; Feng, Q. L.; Cui, F. Z.; Xu, Y. X.; Song, X. H. Int J Biol Macromol 2003, 33, 95.
45. Mi, F.-L.; Sung, H.-W; Shyu, S.-S. Carbohydr Polym 2002, 48, 61.
46. Knaul, J. Z.; Hudson, S. M.; Creber, K. A. M. J Polym Sci B: Polym Phys 1998, 37, 1079.
47. Monteiro, O. A. C.; Airoldi, C. Int J Biol Macromol 1999, 26, 119.
48. Tual, C.; Espuche, E.; Escoubes, M.; Domard, A. J Polym Sci Part B: Polym Phys 2000, 38, 1521.
49. Silva, R. M.; Silva, G. A.; Coutinho, O. P.; Mano J. F.; Reis, R. L. J Mater Sci: Mater Med 2004, 15, 1105.
50. Spasova, M.; Manolova, N.; Paneva, D.; Rashkov, I. e-Polymers 2004, 56, 1.
51. Argüelles-Monal, W.; Goycoolea, F. M.; Peniche, C.; Higuera-Ciapara, I. Polym Gels Networks 1998, 6, 429.
52. Saltzman, W. M. Tissue Engineering: Engineering Principles for the Design of Replacement Organs and Tissues; Oxford University Press: New York, 2004.
53. Koyama, Y.; Taniguchi, A. J Appl Polym Sci 1986, 31, 1951.
54. Bigi, A.; Cojazzi, G.; Panzavolta, S.; Rubini, K.; Roveri, N. Biomaterials 2001, 22, 763.
55. Brandrup, J.; Immergut, E. H.; Grulke, E. A.; Abe, A.; Bloch, D. R.; Polymer Handbook (4th Edition). 2005, John Willey & Sons.